Subfemtosecond dynamics of structural protons in silica xerogels

A. Pietropaolo,[1,*] D. Fernandez-Cañoto,[2,†] E. Perelli-Cippo,[3] S. Dirè,[4] and P. Prosposito[2]

[1]*Dipartimento di Fisica and Centro NAST (Nanoscienze & Nanotecnologie & Strumentazione), Università degli Studi di Romà "Tor Vergata," Via della Ricerca Scientifica 1, 00133, Roma, Italy*

[2]*Dipartimento di Fisica, Università degli Studi di Roma "Tor Vergata," Via della Ricerca Scientifica 1, 00133, Roma, Italy*

[3]*Dipartimento di Fisica "G. Occhialini" and INFM UdR Milano-Bicocca, Università di Milano-Bicocca, Piazza della Scienza 6, 20127 Milano, Italy*

[4]*Dipartimento di Ingegneria dei Materiali e Tecnologie Industriali, Università di Trento, via Mesiano 77, 38050 Trento, Italy*

(Received 4 January 2007; revised manuscript received 4 September 2007; published 14 January 2008)

Deep inelastic neutron scattering measurements on silica xerogels with different geometries (24 and 82 Å pore size diameter) were performed on the VESUVIO spectrometer at the ISIS spallation neutron source, in order to investigate the modification of the ultrashort-time (10^{-15}–10^{-17} s) dynamics of the protons belonging to the silanol groups, when precursors are such as to modify the structural morphology. This paper is also intended to present a complementary experimental technique for the characterization of the microscopic dynamical properties of these materials. The mean kinetic energy $\langle E_k \rangle$ and the momentum distribution $n(p)$ of the protons of the structural silanol groups in the two different systems are derived and compared at the same thermodynamic conditions. The results show that $\langle E_k \rangle$ is different for the two systems, reflecting the differences in the pore morphology. Indeed, $\langle E_k \rangle$ is higher for the system with an average pore diameter of 24 Å, as compared to that of 82 Å.

DOI: 10.1103/PhysRevB.77.014202 PACS number(s): 61.05.fg, 82.70.Gg, 81.05.−t, 78.70.Nx

I. INTRODUCTION

Silica xerogels are porous materials obtained through a procedure known as *sol-gel* that involves the generation of colloidal suspensions (sols) which are subsequently converted to viscous gels and thence to solid materials. These materials have a wide range of application fields, such as insulation,[1] catalysis,[2] controlled drug release,[3] and bioencapsulation,[4] depending on their physical properties and on the variety of nanostructures available. The low cost and high hydrophilicity of these systems could make them useful in proton exchange membrane fuel cells,[5] and can provide much technological fallout in different fields,[6] ranging from coating,[7,8] water repellents for corrosion protection,[9] and biomedical[10] and various electrochemical processes.[11,12]

Until now, the majority of experimental investigations have dealt mostly with structural studies, due to the interesting fractal structure of these amorphous materials[13] and the close correlation between the morphology and physical properties. Dynamical properties have also been studied employing infrared techniques as the diffuse reflectance infrared Fourier transform,[14] Raman spectroscopy,[15] or inelastic neutron scattering measurements.[16–18] Many applications of xerogels rely on their unique surface properties, which are largely determined by the concentration, distribution, and nature of silanols (OH groups attached to the SiO_2 skeleton) on the surface, which have been characterized by employing different NMR techniques,[19–22] infrared[23–25] and Raman[15,26,27] spectroscopic investigations and other analytical tools.[23,28]

Neutron-based techniques are very sensitive to both structure and dynamics of hydrogenous compounds, due to the large scattering cross section of the proton. Besides structural and dynamical investigations at low energy and wave vector transfer, the measurement of the momentum distribution and mean kinetic energy of the structural protons, i.e., the protons belonging to the silanols, has not been done before to our knowledge. The single-proton momentum distribution is of relevant interest, as this physical quantity is strongly related to the local particle's environment, and thus can provide further information on the complex physicochemical characteristics of these systems. Furthermore, this could help in the understanding of the dynamical behavior of water protons adsorbed on silica surfaces.[29]

The single-proton momentum distribution can be measured only through the so-called deep inelastic neutron scattering (DINS),[30] a technique made available since the advent of pulsed neutron sources. In order to satisfy the kinematical constraints to access the DINS regime, i.e., high energy ($\hbar\omega$) and wave vector (q) transfers, epithermal neutrons ($E \geqslant 500$ meV) are indispensable. At high $\hbar\omega$ and q, the scattering can be considered incoherent and occurring on time scales much shorter than the time constants characteristic of the typical collective excitations. This allows the interpretation of the scattering event within the framework of the impulse approximation (IA).[31]

In this paper, we present DINS experiments, carried out on two silica xerogels with different average pore size diameters (24 and 82 Å) in order to monitor the single-particle dynamics. The aim is twofold: (1) to investigate the short-time (10^{-15}–10^{-17} s) dynamics of the protons belonging to the silanol groups, in order to point out the possible modifications of their dynamical response induced by different sol-gel procedures, characterized by different hydrolysis-condensation conditions; (2) to present an experimental tool which can be complementary to the most common characterization techniques, and useful for a comprehensive and thorough description of these interesting porous systems.

This paper is organized as follows. In Sec. II, the theoretical background of DINS is briefly introduced. In Sec. III,

the DINS measurements are briefly described. In Sec. IV, data analysis performed on the DINS experimental measurements is briefly explained, while, in Sec. V, the results are presented and discussed. The conclusions are summarized in Sec. VI. The Appendix reports some details about the synthesis procedure of the two xerogels and gives a brief discussion of the general physicochemical properties of these systems.

II. THEORETICAL FRAMEWORK

In the DINS regime, the inelastic neutron scattering cross section for unpolarized neutrons is related to the dynamic structure factor $S(\mathbf{q},\omega)$ via[32,33]

$$\frac{d^2\sigma(E_0,E_1,2\vartheta)}{d\Omega\, dE_1} = \hbar^{-1}\sqrt{\frac{E_1}{E_0}}[|b|^2 S(\mathbf{q},\omega) + (|b^2| - |b|^2)S_I(\mathbf{q},\omega)], \tag{2.1}$$

b and $S_I(q,\hbar\omega)$ being the scattering length of the probed nucleus and the incoherent contribution to the total dynamic structure factor, respectively. E_0, E_1, and 2ϑ are the incident neutron energy, the scattered neutron energy, and the scattering angle, respectively. At high q values (typically above 20 Å^{-1}), the scattering is incoherent, meaning that it occurs from a single particle. The typical values of the energy transfer $\hbar\omega$ attainable in DINS experiments range from 1 to 100 eV, corresponding to a time scale of the order of 10^{-15}–10^{-17} s, which is much shorter than the characteristic times of the high-energy collective modes in condensed matter (typically well above $\tau \simeq 10^{-15}$ s). Under these kinematical conditions, the nucleus probed by the neutron recoils freely.[30,34] Thus, DINS explores the so-called short-time self-dynamics, and the incoherent and free recoil scattering (resembling that occurring in the Compton scattering of hard x rays off electrons) manifests in the well-known impulse approximation. Within the IA, the inelastic neutron scattering cross section in Eq. (2.1) is.[30,35]

$$\frac{d^2\sigma(E_0,E_1,2\vartheta)}{d\Omega\, dE_1} = \hbar^{-1}\sqrt{\frac{E_1}{E_0}}|b^2|S_{\mathrm{IA}}(\mathbf{q},\omega), \tag{2.2}$$

while the dynamic structure factor is given by[33]

$$S_{\mathrm{IA}}(\mathbf{q},\omega) = \hbar\int n(\mathbf{p})\,\delta\left(\hbar\omega - \hbar\omega_r - \frac{\mathbf{p}\cdot\hbar\mathbf{q}}{M}\right)d\mathbf{p}, \tag{2.3}$$

$n(\mathbf{p})$ being the single-particle momentum distribution. Equation (2.3) establishes that scattering occurs between the neutron and a single particle, while also conserving kinetic energy and momentum of the particle+neutron system. The term $\hbar\omega_r = \hbar^2q^2/2M$ is the recoil energy, i.e., the kinetic energy the struck particle would have, providing it was stationary before the collision and absorbed all the momentum transferred by the neutron. Within the framework of the IA, $\hbar\omega$ and q are explicitly coupled through the West scaling variable y, defined as[32]

$$y = \frac{M}{\hbar^2 q}(\hbar\omega - \hbar\omega_r). \tag{2.4}$$

Equation (2.3) can then be reduced to the form

$$S_{\mathrm{IA}}(\mathbf{q},\omega) = \frac{M}{\hbar q}J(y,\hat{q}), \tag{2.5}$$

where

$$J(y,\hat{q}) = \hbar\int n(\mathbf{p}')\,\delta(\hbar y - \mathbf{p}'\cdot\hat{\mathbf{q}})d\mathbf{p}' \tag{2.6}$$

is the neutron Compton profile (NCP), formally defined as the Radon transform of the momentum distribution. The quantity $\hat{\mathbf{q}}$ is a unit vector, as $J(y,\hat{\mathbf{q}})$ no longer depends on the magnitude of $\mathbf{q}$. The function $J(y,\hat{\mathbf{q}})dy$ is the probability for an atom to have a momentum parallel to $\hat{\mathbf{q}}$ of magnitude between $\hbar y$ and $\hbar(y+dy)$.

For an isotropic system, the direction $\hat{\mathbf{q}}$ is immaterial and Eq. (2.6) becomes[30,36]

$$J(y) = 2\pi\hbar\int_{|\hbar y|}^{\infty} pn(p)dp. \tag{2.7}$$

It has to be stressed that, in the IA framework, $J(y)$ is symmetric and centered at $y=0$ and the relation between $n(p)$ and $J(y)$ is[30,36]

$$n(p) = \frac{1}{2\pi\hbar^3 y}\left(\frac{dJ(y)}{dy}\right)_{hy=p}. \tag{2.8}$$

It is worthwhile mentioning that the IA is strictly valid only in the asymptotic double limit $(q,\hbar\omega)\to\infty$, keeping y constant. For finite values of the energy and wave vector transfers, the longitudinal momentum distribution retains an additional dependence on q which is known as final state effects (FSEs). A detailed description of this contribution can be found in Refs. 37 and 38

III. DINS MEASUREMENTS

DINS measurements on the dried xerogel powders have been carried out at the VESUVIO inverse geometry time-of-flight spectrometer,[39] at the ISIS spallation neutron source (Chilton, United Kingdom). On this instrument a white neutron beam, peaked at about 30 meV and with a $1/E^{0.9}$ tail in the epithermal region, is directed toward the sample position, located at a distance $L_0 \simeq 11$ m (incident flight path) from the 295 K water moderator. The spectrometer was equipped with four banks of ^{6}Li-glass scintillators placed in the angular range $30° \leqslant 2\vartheta \leqslant 60°$ and set up in the resonance filter (RF) configuration.[40] In this setup, the energy of the scattered neutrons was selected by means of filter analyzers, in the form of ^{197}Au metallic foils, that resonantly captured neutrons over narrow energy intervals (resonances). The experimental scattering signal is then reconstructed using the single-difference technique,[41] which accomplishes neutron measurements with and without the filter analyzers placed between the sample and the detectors. Figure 1 shows a schematic drawing of the spectrometer. The experimental signal acquired in the RF configuration on VESUVIO is a time-of-flight spectrum, and the standard expression for the number of neutrons detected in time channel t is given by[42]

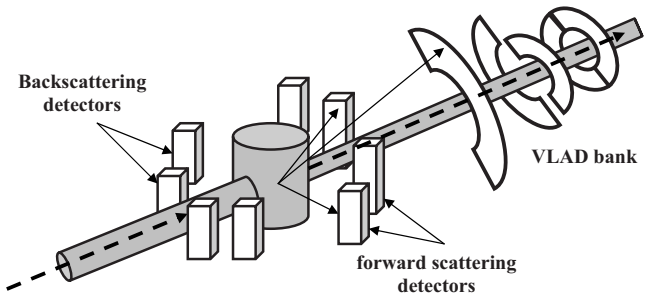

FIG. 1. Schematic drawing of the VESUVIO spectrometer: dashed arrows indicate the incident and the transmitted neutron beams; the continuous arrows represent neutrons scattered toward the ^{6}Li-glass detectors. The very low angle detector (VLAD) bank is shown in the very right-hand side of the drawing.

$$C(t) = 2\hbar\left(\frac{2}{m}\right)^{1/2}\frac{E_0^{3/2}}{L_0}I(E_0)D(E_1)N\frac{d^2\sigma(E_0,E_1,2\vartheta)}{d\Omega\, dE_1}d\Omega, \tag{3.1}$$

where $I(E_0)dE_0$ is the number of neutrons incident with energies between E_0 and E_0+dE_0, $D(E_1)$ is the probability that a scattered neutron of energy E_1 is detected, N is the number of atoms in the beam, and $d\Omega$ is the solid angle subtended by the detector. An assumption made for the IA is that the scattering is incoherent. Hence, if there are different masses present in the sample, the overall count rate is obtained by summing the contribution from each atom of different mass. Therefore, the count rate in Eq. (3.1) can be expressed in terms of the NCP as [see Eqs. (2.2)–(2.5)]

$$C(t) = \frac{E_0 I(E_0)}{\hbar^2 q}\sum_M A_M M J_M(y_M), \tag{3.2}$$

where

$$A_M = \frac{2}{L_0}D(E_1)\sqrt{\frac{2E_1}{m}}d\Omega\, N_M b_M^2, \tag{3.3}$$

$J_M(y_M)$ being the NCP for mass M, and y_M given by Eq. (2.4).

The effect of the instrumental resolution can be taken into account within the *convolution approximation*, where the resolution (mass-dependent) function is incorporated as a single convolution, so that Eq. (3.2) is modified as follows:

$$C(t) = \frac{E_0 I(E_0)}{\hbar^2 q}\sum_M A_M M F_M(y), \tag{3.4}$$

where $F_M(y)=J_M(y)\otimes R_M(y)$ is the convolution of the NCP with the resolution function.

Figure 2 shows three time-of-flight spectra acquired by detectors placed at scattering angles $2\vartheta \simeq 35°$, 50°, and 60°. The peaks at about 320, 225, and 165 μs are the proton recoil signals, measured at a final neutron energy around 4.906 eV (the ^{197}Au resonance), while the one at about 375 μs is the sum of the recoil signals, at the same final neutron energy, from ^{16}O, ^{28}Si, and ^{27}Al nuclei (each contribution being weighted by the scattering cross section of the considered nucleus).

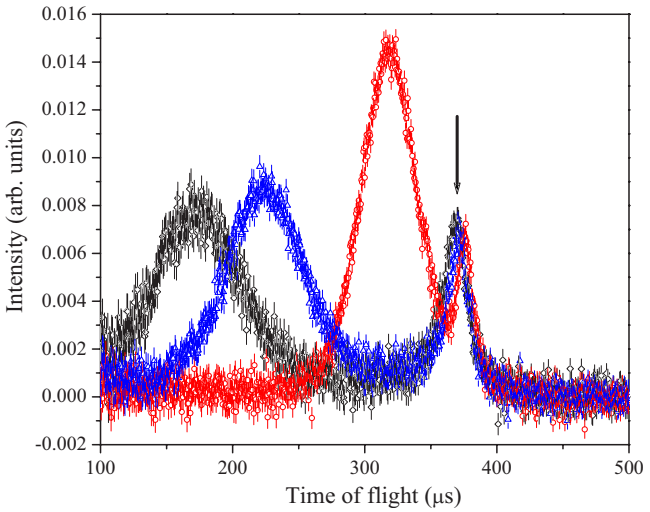

FIG. 2. (Color online) Time-of-flight spectra from the 24 Å pore xerogel, acquired by detector placed at $2\vartheta \simeq 35°$ (open dots), 50° (open triangles), and 60° (open diamonds). The arrow indicates the recoil signal from ^{28}Si+^{16}O+^{27}Al nuclei.

IV. DATA ANALYSIS

The raw time-of-flight spectra have been corrected for multiple scattering[43] and sample container signal, using the standard data reduction procedures employed on VESUVIO.[44,45] After this, the corrected time-of-flight spectra have then been transformed into the *experimental Compton profiles*, $F(y)$ in the y space. The $F(y)$ spectra acquired by detectors at equal (within 1°) scattering angle have been summed in order to enhance statistics. Thus, from the whole set of 32 ^{6}Li-glass detectors, a total of 14 spectra have been obtained and used for the final data analysis. Figure 3 shows an $F(y)$, normalized to unit area, corresponding to the weighted sum of two detectors placed at about 40° scattering angle (the other contributions different from hydrogen being subtracted through the standard data reduction procedures).

The experimental Compton profiles have been fitted, within the *convolution approximation*, using a code based on a FORTRAN 77 routine, employing a MINUIT package[46] for χ^2 minimization. As already pointed out above, the experimental hydrogen recoil spectrum is given by a convolution of the NCP, $J(y)$, and the experimental resolution function $R(y)$. The latter is reconstructed, for each detector, by means of standard calibration procedures.[47] The data fitting procedure envisages the simultaneous fit, in the y domain, of all the experimental Compton profile spectra, employing a single $J(y)$ convoluted with N resolution functions [see Eq. (3.4)], one for each fixed-angle detector. For the present analysis, $J(y)$ was given by the Gram-Charlier series expansion that reads[48,49]

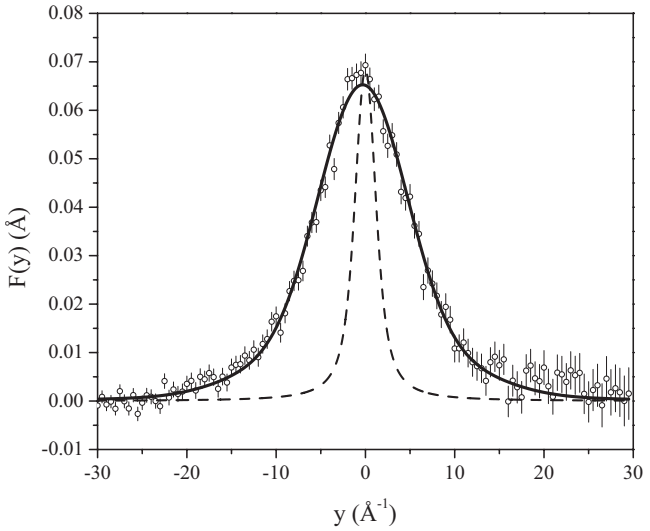

FIG. 3. Experimental Compton profile $F(y)$ (normalized to have unit area) given by the weighted sum of spectra acquired by two detectors at an equal (within 1°) scattering angle of about 40°. The corresponding fit (continuous line) and the resolution function (dashed line) are also shown.

$$J(y) = \frac{e^{-y^2/2\sigma^2}}{\sqrt{2\pi}\sigma}\left[1 + \sum_{n=2} C_{2n} H_{2n}\left(\frac{y}{\sqrt{2}\sigma}\right)\right], \qquad (4.1)$$

where $H_{2n}(y/\sqrt{2}\sigma)$ are Hermite polynomials, and C_{2n} and σ fitting parameters, respectively. The FSEs can be accounted for in Eq. (4.1), by inserting $H_3(y/\sqrt{2}\sigma)$, $H_4(y/\sqrt{2}\sigma)$, and $H_6(y/\sqrt{2}\sigma)$ polynomials with proper q-dependent coefficients.[50,51]

As can be seen, the expansions (4.1) starts with $n=4$: if the second-order polynomial is included in the series, it is overdetermined.[52] In any case we checked, having obtained a fit with this term missing, that including it does not improve the fit significantly.

In the fitting procedure, the entire expression given by Eq. (4.1) plus the additive correction accounting for the FSEs, is convoluted with the instrumental resolution function (one for each detector) and fitted to the data to determine the coefficients in the expansion of the asymptotic $J(y)$ [i.e., Eq. (4.1)]. This procedure (i.e., the *convolution approximation*) is standard on VESUVIO for data analysis on DINS measurements. The errors in the measured $J(y)$ are determined by the uncertainty in the measured coefficients, through their correlation matrix, which is calculated by the fitting program. The uncertainty in the measurement of $J(y)$ at some point y is thus due to the uncertainty in the determined coefficients.

The single-particle mean kinetic energy $\langle E_K \rangle$ is related to the second moment of $J(y)$ and it can be shown that, following Eq. (4.1), it is given by:[30,52]

$$\langle E_K \rangle = \frac{3\hbar^2}{2M}\int_{-\infty}^{\infty} y^2 J(y) dy = \frac{3\hbar^2}{2M}\sigma^2. \qquad (4.2)$$

TABLE I. Summary of the values of σ and $\langle E_K \rangle$ obtained from fitting data on the basis of Eq. (4.1)

ϕ (Å)	σ (Å^{-1})	$\langle E_K \rangle$ (meV)
24	6.90±0.05	296±5
82	6.60±0.08	271±7

The aim of data analysis was to obtain the asymptotic $J(y)$ expressed as a Gaussian function multiplied by a series of Hermite polynomials representing anharmonic contributions, which can provide important experimental details about the environment of the silanol protons.

V. RESULTS AND DISCUSSION

The simultaneous fit over the whole set of spectra considered in the present analysis provided the values $\sigma = 6.90 \pm 0.05$ and 6.60 ± 0.08 Å^{-1} for the xerogels with 24 and 82 Å pore size diameter, respectively. In Table I, the results provided by this analysis are listed. The effect of the resolution tails can be considered almost completely negligible above 10 Å^{-1} (see Fig. 3), as for small masses like proton and deuterium the recoil profile is almost completely dominated by the $n(p)$. It has to be stressed that other systematic effects that could contribute a spurious intensity enhancement, such as the tails of recoil profiles of ^{27}Al+^{28}Si+^{16}O and the multiple scattering, have been corrected by employing the standard data reduction routines available on the VESUVIO instrument. Thus the net effect on the observed intensity of the tails is physically significant.

As a matter of fact, although the convolution approximation has been subjected to different criticisms,[53–55] it has to be stressed that it does not produce any observable net effect on the line shape of the $n(p)$. Indeed, the energy component of the resolution function (i.e., the filter's transfer function) is broadened by the other geometrical components (due to the uncertainties in the flight paths, scattering angles, and time of flight).[56] Indeed, in both the cases where simulations based on Monte Carlo codes, where no convolution is employed (see Refs. 43 and 50), are used to compare simulated and experimental DINS data, and where reference samples are used to reconstruct the resolution functions to be convoluted with the neutron Compton profiles (the standard procedure on VESUVIO), the asymmetric contribution of the Au filter transfer function was found to be not appreciable within the experimental uncertainties. Indeed, the overall spectrometer resolution function at each scattering angle is well reproduced by symmetric functions.[42,47] Other possible effects on the line shape of the proton recoil profile, such as those due to electronic excitations [the so-called non-Born-Oppenheimer (BO) effects], are not appreciable. Indeed, although the existence of sizable non-BO effects in DINS measurements is still highly hypothetical,[57] since their calculation is rather difficult, preliminary attempts on simple systems gave a magnitude of the cross-section deficit far too low to be experimentally detected [see, for example, Ref. 58]. In the present analysis, the only anharmonic term in the

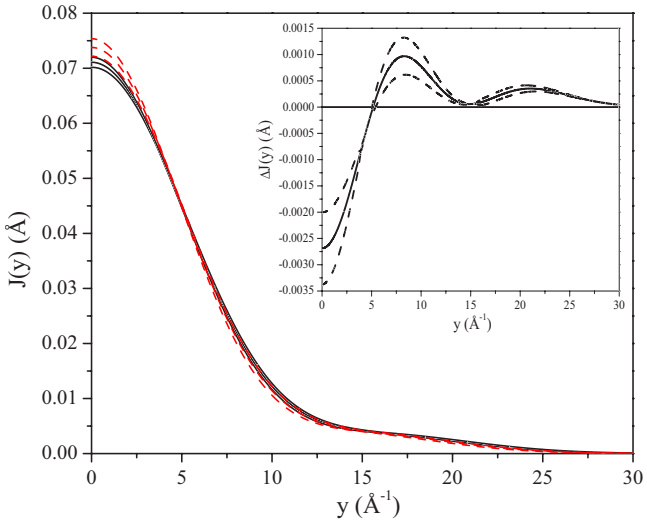

FIG. 4. (Color online) Neutron Compton profiles $J(y)$ and corresponding error bands, relative to protons of the SiOH groups in the 24 Å (continuous lines) and 82 Å (dashed lines) pores. The inset is a blowup of the difference of the two $J(y)$'s, in order to show the differences within the error band.

Gram-Charlier expansion [Eq. (4.1)] that is significant in the fitting procedure is that corresponding to the coefficient C_4, whose values are $C_4=0.612\pm0.0177$ and $C_4=0.588\pm0.0227$ for the xerogel 24 Å and the xerogel 82 Å, respectively.

Figure 4 shows the proton NCPs for both xerogels and their relative difference. The two line shapes are different, within the errors, in almost the whole y range.

The departure from the Gaussian line shape is appreciable and, as a quantitative description, it has to be noted that the excess of kurtosis, defined as

$$\delta = \frac{\mu_4 - 3\mu_2^2}{\mu_2^2}, \tag{5.1}$$

where μ_4 and μ_2 are, respectively, the fourth and the second moment of $J(y)$, is about $\delta_{24\ \text{Å}}=1.85$ and $\delta_{82\ \text{Å}}=1.76$. For a visual and qualitative description, Fig. 5 shows the $J(y)$'s obtained through data fitting and the corresponding Gaussian component graphs.

The area within the full width at half maximum region of the Gauss-Hermite $J(y)$'s is $A_{24\ \text{Å}}\simeq0.713$, while it is $\overline{A}_{24\ \text{Å}}\simeq0.287$ out of this region, while for the other sample the values are $A_{82\ \text{Å}}\simeq0.718$ and thus $\overline{A}_{82\ \text{Å}}\simeq0.282$. The same calculation made on the corresponding Gaussian graphs gives $A_{24\ \text{Å}}\simeq0.760$ and $\overline{A}_{24\ \text{Å}}\simeq0.240$, while for the other system $A_{82\ \text{Å}}\simeq0.756$ and $\overline{A}_{82\ \text{Å}}\simeq0.244$. This indicates that, with respect to the Gaussian case, in the real one there is an enhanced population of high-y states, which provides a further signature of a coherent delocalization effect, as is already pointed out in recent experimental work on DINS measurements from a biological system by Senesi and co-workers.[48]

Figure 6 shows the reconstructed momentum distributions $n(p)$ of the protons in the two xerogels, calculated through Eq. (2.8), while the proton radial momentum distribution

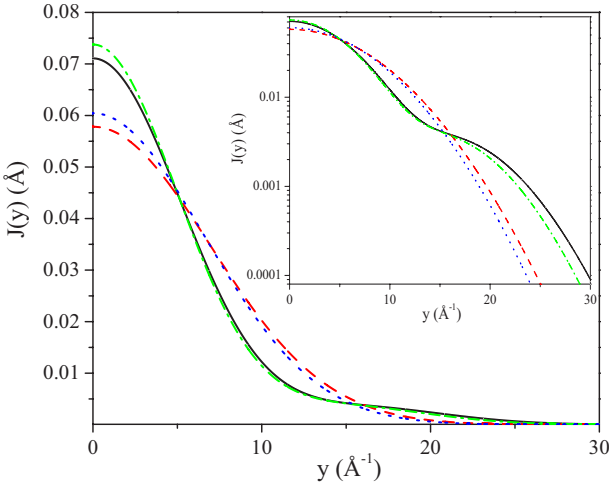

FIG. 5. (Color online) Comparison among the Gauss-Hermite $J(y)$'s obtained through the fitting procedure (continuous and dash-dotted lines) and the corresponding Gaussian component graphs (dashed and dotted lines). The inset shows the same line shapes in a semilogarithmic scale to show the differences on the tails.

$4\pi p^2 n(p)$ (shown as an inset in the figure) highlights the high-p tails in the two cases. The population of the high-p tail is higher, as indicated by the difference in the areas out of the peak maximum, as can be seen in the inset of Fig. 6, where the p value of the shoulder is about 22 Å^{-1} for the 24 Å xerogel, and about 20 Å^{-1} for the 82 Å one.

The momentum distribution $n(p)$ is an exhaustive description of the short-time self-proton-dynamics, subject of the present study. The features shown by the momentum distribution (e.g., anharmonicities) can assess, at least on qualitative grounds, the effects of the local environment on the single-particle subfemtosecond dynamical properties. It has to be stressed that the $J(y)$ [and thus the derived $n(p)$] measured by a DINS experiment on an isotropic sample, such as

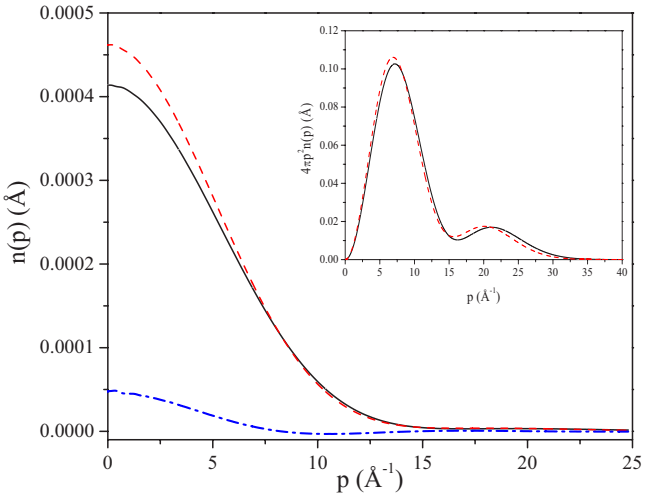

FIG. 6. (Color online) Proton momentum distributions $n(p)$ reconstructed from the NCPs in Fig. 4 following Eq. (2.8) (see text for details) for the 24 Å (continuous line) and 82 Å (dashed line) pores. Their difference (dash-dotted line) is also plotted. The inset plot shows the radial momentum distributions $4\pi p^2 n(p)$.

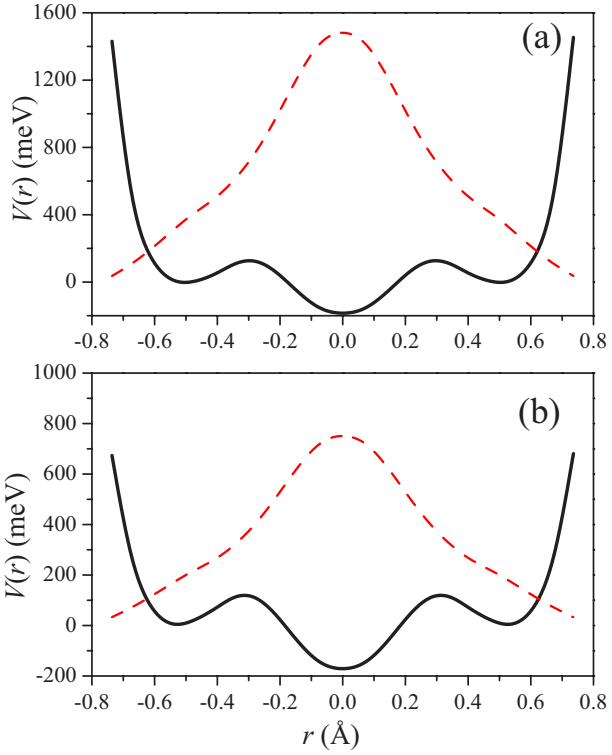

FIG. 7. (Color online) (a) Spherically averaged single-particle potential (continuous line) and corresponding ground state wave function for protons in the xerogel with 24 Å pore size; (b) the same as (a), but for the xerogel with 82 Å pore size.

the xerogel powders investigated in the present work, is a spherically averaged quantity. As already pointed out by Ceperley,[59] $J(y)$ can be related to the single-particle (or one-body) density matrix through the relation

$$J(y) = \frac{1}{\pi}\int_0^\infty dr \cos(ry)n(r). \tag{5.2}$$

In other experimental work, the single-particle effective potential and the ground state wave function have been extracted by employing proper dynamical models.[29,30,52] In the present case, we derived, without employing any model, a spherically averaged (radial) potential $V(r)$ and the corresponding ground state wave function $\psi(r)$. This procedure is presently standard in data analysis on VESUVIO, and the reader is referred to Refs. 30 and 60–62 for a thorough description and for some application examples. Figure 7 shows $V(r)$ and $\psi(r)$ derived for both systems. As can be seen, both potentials strongly depart from a harmonic function, showing an absolute minimum at $r=0$ Å and two symmetric relative minima at $r=\pm 0.55$ Å. The two potentials together with their difference are shown in Fig. 8. The effective potential for the xerogel 24 Å is deeper by about 20 meV and characterized by a first derivative which is, in the whole r region, higher as compared to the 82 Å xerogel. This reflects the difference found between the two $\langle E_k \rangle$ values. Indeed, the proton is more localized in the 24 Å pore, thus showing a higher $\langle E_k \rangle$.

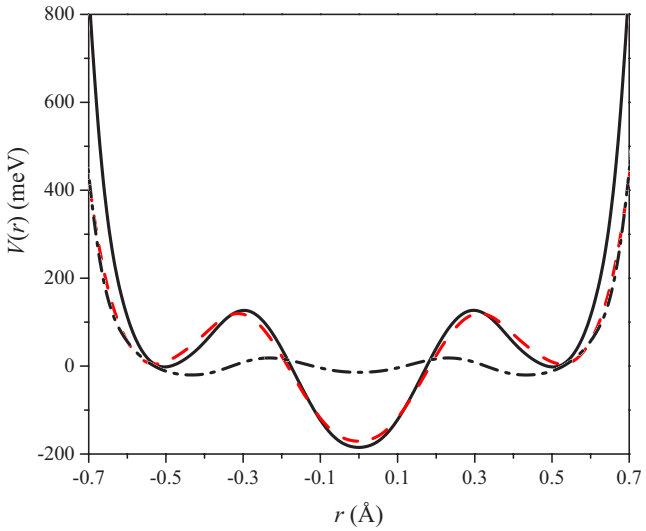

FIG. 8. (Color online) Spherically averaged single-particle potentials for the 24 Å (continuous line) and 82 Å (dashed line) xerogels and their difference (dash-dotted line).

Although less informative than the potential along a given direction, only achievable by a model-dependent approach as already shown for isotropic liquid samples,[29,52] the main features shown by a spherically averaged potential may provide a qualitative description tool for the results obtained. As a final remark, it has to be said that from the properties of the Fourier transform of the Gauss-Hermite functions,[63] it follows that the errors on the potential function $V(r)$ are determined by the errors on the expansion coefficients of $J(y)$ which, as shown in the inset of Fig. 4, differ within the error band.

The close correlation between structural (morphology) and physical (e.g., dynamical) properties, pointed out in numerous works, can provide an interpretation key for the results found for $\langle E_k \rangle$ and $n(p)$ in the two samples. As already assessed in other experimental works (see, for example, Ref. 18), the enhanced surface-to-volume ratio in porous materials can account for the intense interaction at the sample-xerogel interface.[18] The surface-to-volume ratios ϱ are calculated to be $\varrho_{24\ \text{Å}}=2.1\times10^9\ \text{cm}^{-1}$ and $\varrho_{82\ \text{Å}}=4.5\times10^8\ \text{cm}^{-1}$, thus indicating an enhanced interface interaction for the silanols belonging to the smaller-pore xerogel. The surface-to-volume ratio can account for the larger silanol-interface interaction and thus for the higher mean kinetic energy. The origin of the anharmonicities could be related to the coupling of the silanols with the substrate atoms. Such a conclusion is corroborated by other works comparing theoretical and experimental investigations (see Refs. 64 and 65 and references therein) on systems adsorbed on different substrates, where the appreciable coupling of the atoms of the substrate to the adsorbed molecules on the surface was interpreted in terms of anharmonicities of the interatomic bonds of the substrate (nearest-neighbor interactions) affecting the vibrational modes (as well as the other molecular normal modes) of the adsorbed molecules. In the study undertaken in this experimental work, this kind of coupling may be enhanced, as the silanols have to be regarded as a structural

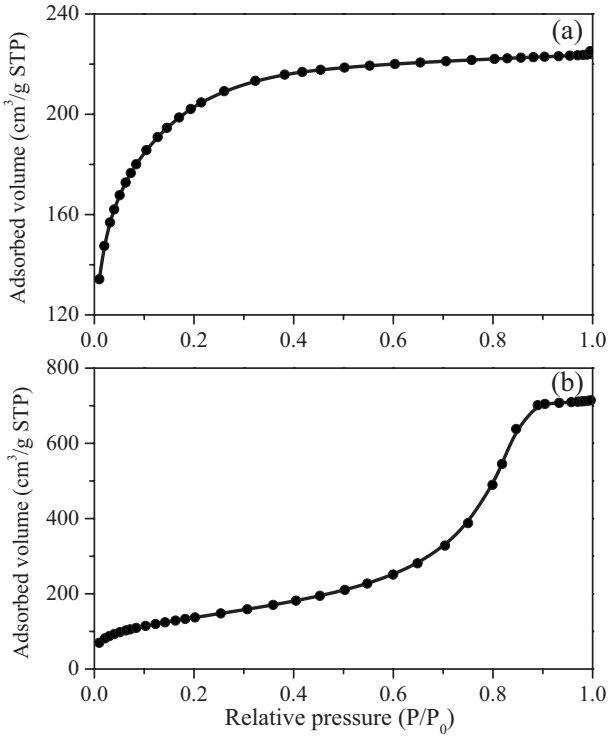

FIG. 9. Nitrogen adsorption isotherm plots at 77 K for the xerogel powder with pore size of (a) 24 and (b) 82 Å.

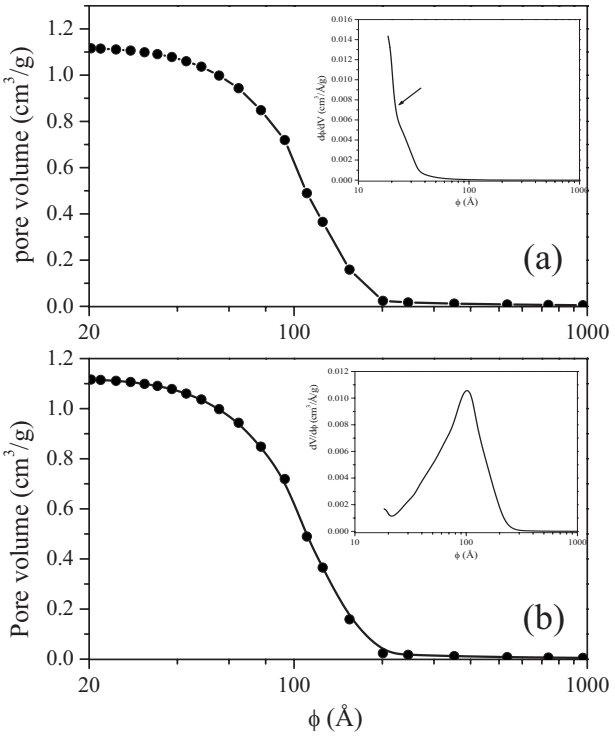

FIG. 10. (a) Adsorption cumulative pore volume distributions as a function of the average pore diameter for the xerogel powder with 24 Å pore distribution; (b) the same as (a) but for the 82 Å pore distribution. In the insets are shown the differential volume distributions for the two powders. The arrow in the inset plot of (a) indicates a discontinuity in the derivative at the value ϕ=24 Å.

component of the SiO_2 matrix rather than considered in the same way as adsorbed molecules. Moreover, the pore topology (e.g., curvature radius and pore size diameter) may enhance the interactions between silanols in such a way that the smaller the pore, the larger the interactions. This may affect the complex coupling and interaction network within the matrix, and in turn can induce appreciable effects on the momentum distribution of the silanol protons, thus giving rise to strongly non-Gaussian $n(p)$.

VI. CONCLUSIONS

Deep inelastic neutron scattering measurements have been performed on two different porous systems, namely, a 24 Å and an 82 Å pore size diameter silica xerogel, obtained from two different sol-gel procedures. The experiment has been carried out at the VESUVIO inverse geometry time-of-flight spectrometer at the ISIS pulsed neutron source, and the measurements allowed us to extract information on the microscopic short-time (10^{-15}–10^{-17} s) dynamics of the protons belonging to the silanol groups of the systems, i.e., proton momentum distribution $n(p)$ and mean kinetic energy $\langle E_k \rangle$. This experiment represents a complementary investigation tool for the direct measurement of microscopic dynamical properties of structural protons within the xerogel skeleton.

Data analysis has been performed within the framework of the impulse approximation, employing an approach relying upon the use of a proton neutron Compton profile given by a Gram-Charlier expansion, where the contribution of anharmonicities can be directly taken into account. It was found that the proton mean kinetic energy is higher for the protons belonging to the silanols of the 24 Å pore size diameter sample as compared to that of the protons in the 82 Å pore size diameter silica xerogel. In both cases, $n(p)$ appreciably departs from a Gaussian distribution.

From the experimental data it was possible to extract the spherically averaged single-particle potential and the corresponding ground state proton wave function. As $\psi(r)$ and $V(r)$ are determined by the proton environment, an explanation of the experimental findings is proposed in terms of a coupling between the silanol normal modes and the anharmonicities of the chemical bonds of the substrate, also correlated with the interactions among the silanols, mostly determined by the pore topology.

This conclusion represents a straightforward extension of the results obtained in the investigations undertaken in different theoretical as well as experimental works. In our opinion, it suggests a possible heuristic explanation and stimulates further discussion, by showing the great potentiality of the DINS technique for a thorough and fine characterization of these interesting porous systems.

ACKNOWLEDGMENTS

This work was supported within the CNR-CCLRC Agreement No. 01/9001 concerning collaboration in scientific research at the spallation neutron source ISIS. The financial support of the Consiglio Nazionale delle Ricerche in this

research is hereby acknowledged. C. Andreani and R. Senesi from Università degli Studi di Roma Tor Vergata (Physics Department) are gratefully acknowledged for discussions during data analysis. S. Schutzmann from Università degli Studi di Roma Tor Vergata (Physics Department) is acknowledged for his collaboration during sample synthesis. One of us (A.P.) gratefully acknowledges G. Paradossi and E. Chiessi from Università degli Studi di Roma Tor Vergata (Dipartimento di Chimica) for interesting discussions.

APPENDIX: SAMPLE PREPARATION

Two xerogel samples were synthesized by a sol-gel procedure, respectively using tetramethoxysilane (TMOS) and tetraethoxysilane (TEOS) as precursors, deionized water, a cosolvent, and an acid catalyst at room temperature.[66] The molar ratios of the solvents and precursor for the first one, named xerogel 24 Å, were $TEOS:H_2O:ethanol=1:10:4$. Nitric acid was added as catalyst to promote hydrolysis of the TEOS precursor. For the second one, labeled xerogel 82 Å, the molar ratios of the components were $TMOS:H_2O:ethanol:HCONH_2=1:10:4:2$. In this case a few drops of polyethylene glycol tetra-octylphenyl ether were also added to the starting solution as surfactant, to avoid cracking and fracturing of large monoliths and improve the quality of the final product. Nitric acid was also added as catalyst. The solutions of the two samples were stirred at room temperature for 30 min and after were poured into Petri dishes covered with aluminum foil. The samples were stored at room conditions and after three months they were dried in the oven at 110 °C for 72 h, in order to eliminate all the residual water. At the end of the synthesis procedure, the samples were carefully ground to a fine powder for the structural characterization and for the neutron scattering measurements. First, the microstructural properties of the xerogel powders were investigated by means of N_2 sorption analysis.[67] N_2 sorption experiments were carried out at 77 K on an ASAP 2010 Micromeritics instrument, and the xerogel samples were degassed below 1.3 Pa. From nitrogen adsorption isotherms, the specific surface area was calculated by the Brunauer-Emmett-Teller equation[68] in the interval $0.05 \leqslant p/p_0 \leqslant 0.33$ with a least squares fit of 0.998. The single-point total pore volume was calculated at $p/p_0=0.995$ and the pore size distribution was obtained using the Barret-Joyner-Halenda model.[69] Figures 9 and 10 show the adsorption isotherms and the pore distribution functions for the two powders, respectively. The main physical characteristics for both samples are reported in Table II. The xerogel 24 Å shows the isotherm curve typical of microporous solids (type I), whereas xerogel 82 Å presents a type IV isotherm.[67] The samples were prepared in the following way for the DINS measurements: they were dried in two different desiccators, at room temperature and under vacuum, employing a P_2O_5 powder. After drying with P_2O_5, the xerogels were inserted into a drying oven at 70 °C for two days, raising the temperature at a gradient of 5 °C/h to avoid structural changes in the skeleton. From the structural and chemical point of view, it has to be considered that the concentration of OH groups at the surface is about 4–5 OH/nm^2 and this quantity can be considered as a physicochemical constant, as it is almost independent of the synthesis conditions.[70] The hydrogen bond interactions of the OH groups at the surface are determined by the Si-O-Si ring size and its opening degree, the number of hydroxyls per silicon site, and the surface curvature.[6] In particular, a small negative curvature radius reduces the distance between neighbor hydroxyls and enhances the hydrogen-bond interaction with respect to a flat surface. Indeed, the interaction among silanols increases as the pore diameter decrease. Porous silica surfaces synthesized through sol-gel procedures are naturally terminated with a variety of surface silanols (isolated, vicinal, and geminal) which are preferential adsorption sites for water molecules. The silanol group is found to dominate the surface chemistry and physics of a variety of adsorbent materials,[71–73] while compounds containing silanol groups, are involved in many industrial processes and synthesis, ranging from formation of silicone polymers to the fabrication of inorganic material through sol-gel processes.[74–77] Silanols are also important for protease inhibition[78] and in the degradation pathway of volatile organosilicon compounds in the atmosphere, that are expected to react with hydroxyl (OH) radicals.[79] Thus, silanols are important in many cases, and the knowledge of their structural and dynamical properties could provide insight into the interpretation of the results of the various processes.

TABLE II. Main physical characteristics of the two silica xerogel samples used for DINS measurements: SSA is the specific surface area, TPV is the total pore volume, and ϕ is the pore diameter. The porosity is also listed in the last column.

Sample	SSA (m^2/g)	TPV (cm^3/g)	ϕ (Å)	Porosity (%)
Xerogel 24 Å	727	0.348	24	50
Xerogel 82 Å	500	1.10	82	73

*Corresponding author; FAX: + 39 06 20235079; antonino.pietropaolo@roma2.infn.it

†Permanent address: Oak Ridge National Laboratory, Oak Ridge, TN 37831, USA.

[1] G. M. Pajonk, Colloid Polym. Sci. **281**, 637 (2003).

[2] T. M. Tillotson and J. G. Reynolds, J. Non-Cryst. Solids **331**, 168 (2003).

[3] P. Kortesuo, M. Haola, M. Kangas, A. Yli-Urpo, J. Kiesavaara, and M. Marvola, Int. J. Pharm. **221**, 107 (2001).

[4] H. R. Luckarift, J. C. Spain, R. R. Naik, and M. O. Stone, Nat. Biotechnol. **22**, 211 (2006).

[5] M. T. Colomer and M. A. Anderson, J. Non-Cryst. Solids **290**, 93

(2001); K. D. Kreuer, Solid State Ionics **97**, 1 (1997).
[6] L. L. Hench, *Sol-Gel Silica: Properties, Processing and Technology Transfer* (Noyes, Bracknell, 1998).
[7] W. A. Finzel and L. M. Parr, J. Water-Borne Coat. **2**, No. 2 (1979).
[8] E. P. Plueddemann, in Proceedings of the 39th Annual Conference, Reinforced Plastic/Composite, The Society of Plastics Industry, 1984 (unpublished).
[9] F. Fracassi, R. d'Agostino, F. Palumbo, E. Angelini, S. Grassini, and F. Rosalbino, Surf. Coat. Technol. **174**, 107 (2003).
[10] T. Yabuta, E. P. Bescher, J. D. Mackenzie, K. Tsuru, S. Hayakawa, and A. Osaka, J. Sol-Gel Sci. Technol. **26**, 1219 (2003).
[11] M. S. Hague, H. A. Naseem, and W. D. Brown, J. Electrochem. Soc. **142**, 3864 (1995).
[12] D. R. Walters, J. Electrochem. Soc. **127**, 2072 (1980).
[13] F. Ferri, B. J. Frisken, and D. S. Cannell, Phys. Rev. Lett. **67**, 3626 (1991).
[14] A. Fidalgo and L. M. Ilharco, J. Non-Cryst. Solids **347**, 128 (2004).
[15] A. Anedda, C. M. Carbonaro, F. Clemente, R. Corpino, and P. C. Ricci, J. Phys. Chem. B **107**, 13661 (2003).
[16] U. Buchenau, M. Prager, N. Nucker, A. J. Dianoux, N. Ahmad, and W. A. Phillips, Phys. Rev. B **34**, 5665 (1986).
[17] U. Buchenau, H. M. Zhou, N. Nucker, K. S. Gilory, and W. A. Phillips, Phys. Rev. Lett. **60**, 1318 (1988).
[18] D. W. Brown, P. E. Sokol, and S. A. FitzGerald, Phys. Rev. B **59**, 13258 (1999).
[19] J. Köler, D. B. Chase, R. D. Farlee, A. J. Vega, and J. J. Kirkland, J. Chromatogr. **352**, 275 (1986).
[20] V. Y. Davidov, H. Pfeifer, and I. Junger, Russ. J. Phys. Chem. **57**, 1527 (1983).
[21] C. E. Bronnimann, R. C. Zeigler, and G. E. Maciel, J. Am. Chem. Soc. **110**, 2023 (1988).
[22] G. E. Maciel and D. W. Sindorf, J. Am. Chem. Soc. **102**, 7606 (1980).
[23] T. A. Guiton and C. G. Pantano, Colloids Surf., A **74**, 33 (1993).
[24] R. M. Almeida, T. A. Guiton, and C. G. Pantano, J. Non-Cryst. Solids **121**, 193 (1990).
[25] P. Innocenzi, J. Non-Cryst. Solids **316**, 309 (2003).
[26] C. J. Brinker and G. W. Sherer, *Sol-Gel Science* (Academic Press, San Diego 1990).
[27] B. A. Morrow and R. A. McFarlane, J. Chem. Phys. **90**, 3192 (1986).
[28] R. S. Mikhail and E. Robens, *Microstructure and Thermal Analysis of Solid Surfaces* (John Wiley & Sons, New York, 1983).
[29] V. Garbuio, C. Andreani, S. Imberti, A. Pietropaolo, G. F. Reiter, and R. Senesi, J. Chem. Phys. **127**, 154501 (2007).
[30] C. Andreani, D. Colognesi, J. Mayers, G. F. Reiter, and R. Senesi, Adv. Phys. **54**, 377 (2005).
[31] P. M. Platzman and N. Tzoar, Phys. Rev. **139**, A410 (1965); E. Pace, G. Salmé, and G. West, Phys. Lett. B **273**, 205 (1991); P. Eisenberger and P. M. Platzman, Phys. Rev. A **2**, 415 (1970).
[32] *Momentum Distributions*, edited by R. N. Silver and P. E. Sokol (Plenum, New York, 1989).
[33] S. W. Lovesey, *Theory of Neutron Scattering from Condensed Matter*, 3rd ed. (Oxford University Press, Oxford, 1987).
[34] G. Watson, J. Phys.: Condens. Matter **8**, 5955 (1996).
[35] R. Scherm, Ann. Phys. (Paris) **7**, 349 (1972).
[36] C. Andreani, A. Filabozzi, E. Pace, and J. Mayers, Phys. Rev. B **54**, 6255 (1996).
[37] R. N. Silver, Phys. Rev. B **37**, 3794 (1988).
[38] R. N. Silver, Phys. Rev. B **39**, 4022 (1989).
[39] R. Senesi, C. Andreani, Z. Bowden, D. Colognesi, E. Degiorgi, A. L. Fielding, J. Mayers, M. Nardone, J. Norris, M. Praitano, N. J. Rhodes, W. G. Stirling, J. Tomkinson, and C. Uden, Physica B **276-278**, 200 (2000).
[40] M. P. Paoli *et al.*, in ICANS VIII—Proceedings of the Eighth Meeting of the International Collaboration on Advanced Neutron Sources, Rutherford Appleton Laboratory Report No. RAL-85-110, 1985, p. 577 (unpublished).
[41] R. J. Newport, M. P. Paoli, V. T. Pugh, R. N. Sinclair, A. D. Taylor, and W. G. Williams, in ICANS VIII—Proceedings of the Eighth Meeting of the International Collaboration on Advanced Neutron Sources (Ref. 40), p. 562.
[42] C. Andreani, D. Colognesi, E. Degiorgi, A. Filabozzi, M. Nardone, E. Pace, A. Pietropaolo, and R. Senesi, Nucl. Instrum. Methods Phys. Res. A **497**, 535 (2003).
[43] J. Mayers, A. L. Fielding, and R. Senesi, Nucl. Instrum. Methods Phys. Res. A **481**, 454 (2002).
[44] C. Andreani, D. Colognesi, E. Degiorgi, and M. A. Ricci, J. Chem. Phys. **115**, 11243 (2001).
[45] C. Andreani, E. Degiorgi, R. Senesi, F. Cilloco, D. Colognesi, J. Mayers, M. Nardone, and E. Pace, J. Chem. Phys. **114**, 387 (2001).
[46] F. James, Computer code MINUIT (CERN Program Library, Geneva, 1994).
[47] A. L. Fielding, J. Mayers, Nucl. Instrum. Methods Phys. Res. A **480**, 680 (2002).
[48] R. Senesi, A. Pietropaolo, A. Bocedi, S. E. Pagnotta, and F. Bruni, Phys. Rev. Lett. **98**, 138102 (2007).
[49] V. F. Sears, Phys. Rev. **185**, 200 (1969).
[50] R. Senesi, D. Colognesi, A. Pietropaolo, and T. Abdul-Redah, Phys. Rev. B **72**, 054119 (2005).
[51] V. F. Sears, Phys. Rev. B **30**, 44 (1984).
[52] G. F. Reiter, J. C. Li, J. Mayers, T. Abdul-Redah, and P. Platzman, Braz. J. Phys. **34**, 142 (2004).
[53] J. J. Blostein, J. Dawidowski, and J. R. Granada, Nucl. Instrum. Methods Phys. Res. B **217**, 333 (2004); J. J. Blostein, J. Dawidowski, and J. R. Granada, Phys. Rev. B **71**, 054105 (2005).
[54] C. A. Chatzidimitriou-Dreismann, T. A. Redah, R. M. F. Streffer, and J. Mayers, Phys. Rev. Lett. **79**, 2839 (1997).
[55] E. B. Karlsson, C. A. Chatzidimitriou-Dreismann, T. Abdul-Redah, R. M. F. Streffer, B. Hjrvarsson, J. Öhrmalm, and J. Mayers, Europhys. Lett. **46**, 617 (1999).
[56] C. Andreani, G. Baciocco, R. S. Holt, and J. Mayers, Nucl. Instrum. Methods Phys. Res. A **276**, 297 (1989).
[57] I. Gidopoulos, Phys. Rev. B **71**, 054106 (2005); G. F. Reiter and P. M. Platzman, *ibid.* **71**, 054107 (2005).
[58] (a) R. A. Cowley, J. Phys.: Condens. Matter **15**, 4143 (2003); (b) D. Colognesi, Physica B **344**, 73 (2003).
[59] D. M. Ceperley, in *Momentum Distributions*, edited by R. N. Silver and P. E. Sokol (Plenum Press, New York, 1989).
[60] G. F. Reiter, C. Burnham, D. Homouz, P. M. Platzman, J. Mayers, T. Abdul-Redah, A. P. Moravsky, J. C. Li, C. K. Loong, and A. I. Kolesnikov, Phys. Rev. Lett. **97**, 247801 (2006).
[61] Yejun Feng, C. Ancona-Torres, T. F. Rosenbaum, G. F. Reiter, D. L. Price, and E. Courtens, Phys. Rev. Lett. **97**, 145501 (2006).
[62] G. F. Reiter, J. Mayers, and P. Platzman, Phys. Rev. Lett. **89**, 135505 (2002).
[63] M. K. Atakishiyeva and N. M. Atakishiyev, J. Phys. A **30**, 559

(1997).
[64] Y. Zhen and P. Piercy, Phys. Rev. B **47**, 9797 (1993).
[65] B. N. J. Persson and R. Ryberg, Phys. Rev. B **40**, 10273 (1989).
[66] R. F. Silva and W. L. Vasconcelos, Mater. Res. **2**, 197 (1999).
[67] J. Rouquerol, F. Rouquerol, and K. S. W. Sing, *Adsorption in Powders and Porous Solids: Principles, Methodology and Applications* (Academic Press, New York, 1999).
[68] S. Brunauer, P. H. Emmett, and E. Teller, J. Am. Chem. Soc. **60**, 309 (1938).
[69] E. P. Barret, L. G. Joyner, and P. P. Halenda, J. Am. Chem. Soc. **73**, 373 (1951).
[70] L. T. Zhuraley, Pure Appl. Chem. **61**, 1969 (1989).
[71] F. Schüth, K. S. W. Sing, and J. Weithamp, *Handbook of Porous Solids* (Wiley/VCH, Weinheim, 2002), Vols. 1–5.
[72] R. T. Yang, *Adsorbents: Fundamentals and Applications* (Wiley/Interscience, New York, 2003).
[73] A. P. Legrand, *The Surface Properties of Silicas* (Wiley/Interscience, New York, 1998).
[74] V. Chandrasekhar, R. Boomiskankar, and S. Nagedran, Chem. Rev. (Washington, D.C.) **104**, 5847 (2004).
[75] A. L. Smith, *The Analytical Chemistry of Silicones* (Wiley/Interscience, New York, 1991).
[76] P. D. Lickiss, Adv. Inorg. Chem. **42**, 147 (1995).
[77] R. Murugavel, A. Voigt, R. G. Walawalkar, and H. W. Roesky, Chem. Rev. (Washington, D.C.) **96**, 2205 (1996).
[78] M. Wa Mutahi, T. Nittoli, L. Guo, and S. McN. Sieburth, J. Am. Chem. Soc. **124**, 7363 (2002).
[79] E. C. Tuazon, S. Aschmann, and R. Atkinson, Environ. Sci. Technol. **34**, 1970 (2000).